Chinese Journal of Catalysis 41 (2020) 1715–1722

available at www.sciencedirect.com

ScienceDirect

journal homepage: www.elsevier.com/locate/chnjc

Article

Cu-SAPO-17: A novel catalyst for selective catalytic reduction of NO_x

Xiaona Liu [a,b], Yi Cao [a,c], Nana Yan [a,b], Chao Ma [a,b,d], Lei Cao [a], Peng Guo [a,*], Peng Tian [a,#], Zhongmin Liu [a,$]

[a] *National Engineering Laboratory for Methanol to Olefins, State Energy Low Carbon Catalysis and Engineering R&D Center, Dalian National Laboratory for Clean Energy, Dalian Institute of Chemical Physics, Chinese Academy of Sciences, Dalian 116023, Liaoning, China*

[b] *University of Chinese Academy of Sciences, Beijing 100049, China*

[c] *School of Material Science and Chemical Engineering, Ningbo University, Ningbo 315211, Zhejiang, China*

[d] *Zhang Dayu School of Chemistry, Dalian University of Technology, Dalian 116024, Liaoning, China*

ARTICLE INFO

Article history:
Received 21 February 2020
Accepted 29 March 2020
Published 5 November 2020

Keywords:
SAPO-17 molecular sieve
Rietveld refinement
Host-guest interaction
Selective catalytic reduction by ammonia (NH_3-SCR)
Hydrothermal stability
Location of Cu^{2+}

ABSTRACT

The high-temperature (HT) and low-temperature (LT) hydrothermal stabilities of molecular-sieve-based catalysts are important for the selective catalytic reduction of NO_x with ammonia (NH_3-SCR). In this paper, we report a catalyst, Cu^{2+} loading SAPO-17, synthesized using cyclohexylamine (CHA), which is commercially available and inexpensive and is utilized in NH_3-SCR reduction for the first time. After systematic investigations on the optimization of Si and Cu^{2+} contents, it was concluded that Cu-SAPO-17-8.0%-0.22 displays favorable catalytic performance, even after being heated at 353 K for 24 h and at 973 K for 16 h. Moreover, the locations of CHAs, host–guest interaction and the Brönsted acid sites were explored by Rietveld refinement against powder X-ray diffraction data of as-made SAPO-17-8.0%. The refinement results showed that two CHAs exist within one *eri* cage and that the protonated CHA forms a hydrogen bond with O4, which indicates that the proton bonding with O4 will form the Brönsted acid site after the calcination.

1. Introduction

With a heightened sense of awareness of the environment, emission regulations have become extremely stringent. NO_x can contribute to the formation of photochemical smog, acid rain, haze etc, Thus, one of the most important aspects of these regulations is to lower NO_x emissions [1,2]. Until now, selective catalytic reduction by ammonia (NH_3-SCR) was considered an effective technique to eliminate NO_x in the lean-burn condition [1,2]. In a typical diesel emission after-treatment system, diesel particle filters (DPFs) are generally placed beneath the NH_3-SCR catalyst to trap particulate matter (PM). The regeneration process requires the DPFs to be heated to a high temperature (usually >873 K) [3]. Moreover, the SCR catalyst is often exposed at low temperatures (usually <373 K) during the diesel storage and its cold-start period. Thus, the NH_3-SCR catalyst needs to have both excellent high-temperature (HT) and low-temperature (LT) hydrothermal stabilities and catalytic performance.

Thus far, Cu-exchanged zeolites, such as Cu-beta (Frame-

* Corresponding author. Tel: +86-411-84379149; Fax: +86-411-84379289; E-mail: pguo@dicp.ac.cn
# Corresponding author. Tel: +86-411-84379218; Fax: +86-411-84379289; E-mail: tianpeng@dicp.ac.cn
$ Corresponding author. Tel: +86-411-84379998; Fax: +86-411-84379289; E-mail: liuzm@dicp.ac.cn
This work was supported by the National Natural Science Foundation of China (21972136, 21676262, 21606221, 21991091) and the Key Research Program of Frontier Sciences, CAS (QYZDB-SSW-JSC040).
DOI: 10.1016/S1872-2067(20)63609-9 | http://www.sciencedirect.com/science/journal/18722067 | Chin. J. Catal., Vol. 41, No. 11, November 2020

work type code (FTC): ***BEA**) [1,2,4], Cu-ZSM-5 (**MFI**) [1,2,5], Cu-SSZ-13 (**CHA**) [1–3,6], Cu-SSZ-39 (**AEI**) [1,7], Cu-LTA (**LTA**) [8], Cu-SSZ-16 (**AFX**) [9], and Cu-SAPO-34 (**CHA**) [1,3], have been considered as promising NH_3-SCR catalysts. Among these, silicoaluminophosphate (SAPO)-based catalysts are attracting increasing attention owing to their excellent HT hydrothermal stability. To our knowledge, among the 41 SAPO molecular sieves (MSs) [10], only Cu-SAPO-34 (**CHA**), Cu-SAPO-18 (**AEI**) [11], Cu-SAPO-35 (**LEV**) [12], MnO_x-SAPO-11 (**AEL**) [13], and Cu-SAPO STA-7 (**SAV**) [14] have been used as NH_3-SCR catalysts. With the exception of SAPO-11, the others have similar structural features: small pore openings and large cages that show promising NO_x conversion. However, SAPOs are known to exhibit LT hydrothermal instability. Therefore, it motivates researchers to explore other small pore sieves with both HT and LT hydrothermal stability characteristics. Apart from the aforementioned small pore SAPO MSs, SAPO-17 (FTC: **ERI**) is another small pore cage-based MS that might be a potential NH_3-SCR catalyst.

SAPO/AlPO-17 has a three-dimensional (3D) 8 × 8 × 8 ring channel system [15]. It consists of *eri*-cage (Fig. 1a) and *can-d6r* columns (Fig. 1b) running along the *c*-axis. Each *can-d6r* column links with six similar columns, creating large ellipsoidal *eri* cages (6.79 × 12.07 Å) (Fig. 1c). SAPO/AlPO-17 can be synthesized using a variety of organic structure directing agents (OSDAs), such as piperidine (PI) [15], quinuclidine [16], cyclohexylamine (CHA) [17–19], neopentylamine [20], methylamine [21], *N,N,N′,N′*-tetramethyl-1,6-hexanediamine (TMHD) [22], *N,N,N,N′,N′,N′*-hexamethyl hexamethylene hydroxide [23], and 1,4-bis (*N*-methylpyrrolidinium) butane hydroxide [24].

Knowledge of the locations of OSDAs within cages and the host (framework)-guest (OSDA) interactions can provide indirect information regarding Brönsted acid sites [25]. Additionally, this knowledge might provide the possible locations of exotic active sites such as Cu^{2+} for NH_3-SCR. Molecular modelling [26], spectroscopic characterization (UV-Raman, NMR, and IR) [27–29], and refinement against diffraction data (X-ray, electron, and neutron) [25,30,31] can be used to determine the locations of the guest species. Compared with other methods, Rietveld refinement against powder X-ray diffraction (PXRD) not only provides the atomic coordinates of guest species and the host framework, but also considers the effects arising from the synthesis condition (such as different types of silica precursors). For example, the structural features of OSDA directing DNL-6, a novel small pore **RHO**-type SAPO material, have been explored using Rietveld refinement; subsequently, the targeted synthesis of DNL-6 using a series of predicted OSDAs has been accomplished [32]. Therefore, Rietveld refinement is an appropriate method to investigate the locations of OSDAs in SAPO/AlPO-17. Thus far, Joseph J. Pluth and Alain Tuel *et al* have utilized single-crystal X-ray diffraction (SXRD) to investigate the precise locations of PI and TMHD in AlPO-17 [15,22]. The exact positions of other OSDAs in SAPO/AlPO-17 remain undiscovered.

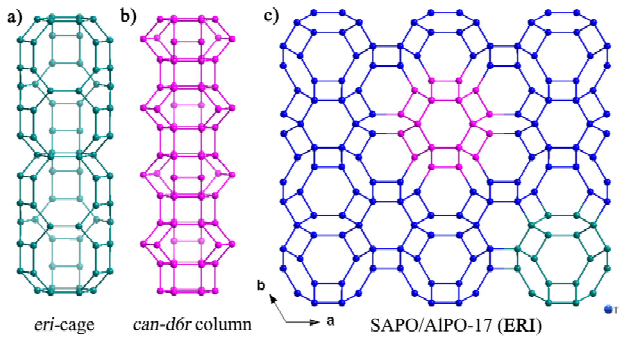

Fig. 1. a) *eri*-cage and b) *can-d6r* column running along the *c*-axis, highlighted in green and pink, respectively; c) **ERI**-type framework viewed along the *c*-axis. For clarity, O atoms are omitted.

In this study, we synthesized SAPO-17 with tunable Si contents (the samples are denoted as SAPO-17-m, where m indicates Si/(Si+Al+P)) by using commercially available, inexpensive CHA as OSDA, and we investigated their locations, host-guest interactions, and Brönsted acid sites through Rietveld refinement against PXRD data. Moreover, we explored the NH_3-SCR activities of Cu-SAPO-17 with different Si and Cu contents; the catalysts were denoted as Cu-SAPO-17-*m*-*n*, where *m* and *n* indicate Si/(Si+Al+P) and Cu/Si, respectively. Among these catalysts, Cu-SAPO-17-8.0%-0.22 displays favorable catalytic performance and HT and LT hydrothermal stability characteristics.

2. Experimental

2.1. Materials

Pseudo-boehmite (66.5%), aluminium isopropoxide (Aladdin, ≥ 98%), phosphoric acid (80%), Fumed silica (FS, CAB-O-SIL M-5), colloidal silica (CS, 27.34%), tetraethylorthosilicate (TEOS, Kermel, ≥ 98%), cyclohexylamine (CHA, Sinopharm Chemical Reagent, ≥ 99%), aluminum nitrate (Sinopharm Chemical Reagent, ≥ 99%), sodium hydroxide (Aladdin, ≥ 99%), potassium hydroxide (Damao Chemical Reagent Factory, ≥ 85%), potassium chloride (Kermel, ≥ 99%), and hydrofluoric acid (Damao Chemical Reagent Factory, 40%) were used as received. 1,4-bis (*N*-methylpyrrolidinium) butane bromide (1,4-$MPBr_2$) was synthesized according to reference [33].

2.2. Zeolite synthesis

2.2.1. Synthesis of heterogeneous seeds (aluminosilicate zeolite with *ERI* topology)

Fumed silica was added to the solution containing aluminum nitrate, sodium hydroxide, potassium hydroxide and 1,4-$MPBr_2$. When the mixture formed a homogeneous gel with the composition of 30 SiO_2: 0.5 Al_2O_3: 15 NaOH: 15 KOH: 4.5 1,4-$MPBr_2$: 1191 H_2O, it was transferred to a stainless-steel autoclave and crystallized at 433 K for 110 h. The product was obtained by centrifugation, washed with deionized water, and dried at 373 K overnight. The heterogeneous seeds were obtained by calcinating the as-made sample at 873 K for 4 h and exchanged with 1 M NH_4NO_3 solution at 353 K for 2 h (repeat three times).

2.2.2. Synthesis of SAPO-17

SAPO-17 was synthesized according to the previously reported procedure [34,35]. The gel compositions are listed in Table S1, and the gel is prepared by the following procedure. An aluminium source (pseudo-boehmite or aluminium isopropoxide) and phosphoric acid were mixed with deionized water for 2 h, and a silica source (colloidal silica or aluminosilicate zeolite), CHA, HF, and KCl were added to the mixture stirred until the gel was homogeneous. Finally, seeds were added to the gel and stirred for another 30 min. The mixture was transferred to a stainless-steel autoclave and crystallized at 473 K for a known time. In all cases, the products were obtained by centrifugation, washed with deionized water, and dried overnight at 373 K.

2.2.3. Synthesis of Cu-SAPO-17

Cu-SAPO-17 was prepared according to the previous reported method [36]. The as-made samples were exchanged with appropriate Cu in the aqueous solution of cupric acetate monohydrate at 353 K for 4 h. The Cu contents of Cu-SAPO-17 were measured by XRF and the results are listed in Table 1. When testing the NH_3-SCR activities, Cu-SAPO-17 samples were calcined at 873 K for 2 h.

2.3. Characterization

The powder X-ray diffraction (PXRD) data for phase identification was collected on a PANalytical X'Pert PRO X-ray diffractometer (Cu K_α, λ = 1.5418Å). PXRD data (2θ ranges from 5° to 120°) used for the Rietveld refinement was recorded on the high-resolution STOE STADI P ESSENTIAL diffractometer equipped with a Mythen ll detector in the Debye-Scherrer mode (Cu $K\alpha_1$, λ = 1.5406 Å). The diameter of the capillary is 0.2 mm. Scanning emission microscope (SEM) images were performed on a Hitachi SU8020 microscope. PANalytical Axios advanced X-ray fluorescence spectroscopy (XRF) was used to determine the content of Si, Al, P, Cu, Na, and K. Thermogravimetry analysis (TGA) was performed on a TA Q-600 analyzer at a rate of 10 K/min from room temperature to 1173 K.

The in-situ diffuse reflectance infrared Fourier transform (DRIFT) spectra were measured on a Bruker Vertex 70. Undiluted samples were used to investigate the vibrations of CHAs. To eliminate the effect of adsorbed water prior to collecting the spectrum at 473 K in a N_2 stream, the samples were dried at 473 K for 1 h in the presence of N_2 (50 mL/min).

Table 1
Cu contents of Cu-SAPO-17.

Sample	Cu content[a] (wt%)	Cu^{2+} content[b] (wt%)
Cu-SAPO-17-2.7%-0.42	1.17	0.31
Cu-SAPO-17-5.0%-0.47	2.30	0.46
Cu-SAPO-17-8.0%-0.43	3.34	0.58
Cu-SAPO-17-8.0%-0.11	0.90	0.40
Cu-SAPO-17-8.0%-0.22	1.82	0.53
Cu-SAPO-17-8.0%-0.22-HT aged	—	0.49
Cu-SAPO-17-8.0%-0.22-LT aged	—	0.51

[a] Determined by XRF.
[b] Quantified by EPR results.

The NH_3-IR spectra were recorded on Bruker Tensor 27 spectrometer in the frequency range 4000–800 cm^{-1} with a resolution of 4 cm^{-1}. Prior to the experiments, catalysts were heated to 773 K under vacuum and maintained at this temperature for 1 h. Eventually, they cooled down to 423 K and adsorbed NH_3 at this temperature for 30 min. Finally, spectrum was recorded after desorbing NH_3 at 473 K for 40 min.

The N_2 adsorption experiments were performed on Micrometrics ASAP 2020 analyzer. Prior to the test, samples were degassed at 623 K for 4 h. NH_3-TPD was recorded on Micromeritics AutoChedm II chemisorption analyzer. Before the test, samples were heated to 873 K and maintain at this temperature for 30 min in the presence of He. Then samples were cooled down to 423 K, adsorbed NH_3 at this temperature for 30 min, and purged by He for another 30 min. Finally, samples were heated to 923 K with a rate of 10 K/min and TCD was used to detect the signals.

The solid-state MAS NMR experiments were recorded on a Bruker Avance lll 600 spectrometer equipped with a 14.1 T wide-bore magnet using a 4 mm WVT probe. The resonance frequencies of ^{1}H, ^{13}C, ^{29}Si, ^{27}Al, and ^{31}P are 600.13 MHz, 150.9 MHz, 119.2 MHz, 156.4 MHz, and 242.93 MHz, respectively. ^{13}C MAS NMR spectra and ^{29}Si MAS NMR spectra were recorded using cross-polarization (CP, ^{1}H-^{13}C, and ^{1}H-^{29}Si) sequence at the spinning rate of 12 kHz and 8 kHz, respectively. The chemical shifts were referenced to adamantine and 4,4-dimethyl-4-silapentane sulfonate sodium salt at 29.5 ppm, 0 ppm, respectively. ^{27}Al MAS NMR and ^{31}P MAS NMR were recorded with a spinning rate of 12 kHz. Chemical shifts of ^{27}Al MAS NMR and ^{31}P MAS NMR were referenced to $(NH_4)Al(SO_4)_2$ $12H_2O$ and diammonium phosphate at −0.4 ppm and 1.13 ppm, respectively.

The UV-vis spectrum was collected on Varian Cary 5000 UV-Vis-NIR spectrophotometer and $BaSO_4$ was used as a reference.

Electron paramagnetic resonance (EPR) spectrum was recorded on Bruker A 200 at 77 K to identify the isolated Cu^{2+}. Before the test, samples were treated by N_2 at 285 K for 12 h. $CuSO_4$ solution was used to quantify the isolated Cu^{2+}.

2.4. High-temperature (HT) and low-temperature (LT) hydrothermal treatment

HT hydrothermal aging was performed at 973 K for 16 h in the presence of 10% H_2O in air.

LT hydrothermal aging was performed at 353 K for 24 h in the presence of 10% H_2O in N_2 atmosphere.

2.5. Catalytic activity test

The NH_3-SCR activity was performed in a fixed bed with the gas hourly space velocity (GHSV) of 90,000 h^{-1}. 100 mg catalyst (60–80 mesh) mixed with 200 mg quartz beads (60–80 mesh) was transferred to a quartz tubular reactor. Prior to testing the activity, the catalyst was heated to 823 K (2 K/min) and maintained at this temperature for 30 min in the presence of feed gases. Then, the catalyst was cooled down gradually to 426 K

and started to test. The feed gases are balanced by N_2 and the final component is 0.05% NO, 0.05% NH_3, 6.1% O_2, and 6.4% H_2O. Fourier transform infrared (FTIR) spectrometer (Tensor 27, Bruker) was used to detect NO, NO_2, and N_2O in the inlet and outlet gases.

3. Results and discussion

3.1. Characterization of SAPO-17 molecular sieves

The PXRD data (Fig. 2), scanning electron microscopy (SEM) images (Fig. S1), and BET results (Table S2) demonstrate the high crystallinity of SAPO-17. X-ray fluorescence spectroscopy (XRF) is used to determine the contents of Si, Al, P, and Cu, while the number of CHA and H_2O is obtained via thermo gravimetric analysis (TG) (Fig. S2). The obtained unit-cell chemical compositions and Cu contents are listed in Table 1 and S2. ^{1}H-^{29}Si CP MAS NMR spectrum (Fig. S3) indicates that all three samples contain silicon islands. Peaks at −20.2, −26.9, and −31.3 ppm in the ^{31}P NMR spectrum (Fig. S4) can be assigned to different local environments of tetrahedral phosphorus in the framework [18]. The peak at 15.2 ppm in ^{27}Al NMR spectrum (Fig. S5) belongs to a portion of five-coordinated Al1 interacting with hydroxyl groups, while 35.2 and 43.8 ppm are assigned to tetrahedral Al2 and Al1, respectively [18]. The spectrum of ^{1}H-^{13}C CP MAS NMR (Fig. 3) shows peaks at 26.94, 27.67, 34, and 56 ppm, indicating that the CHAs remain intact and protonated [18]. These results are also confirmed using in-situ DRIFT. As illustrated in Fig. 4, the bands at 3222, 1600, and 1502 cm^{-1} are assigned to the stretching and deformation vibration of NH_3^+, indicating that CHAs are protonated [19]. It is notable that there is a sharp peak at 3629 cm^{-1}, signifying the presence of extra framework OH^- [19], which is consistent with the ^{27}Al NMR result. Although these results indicate that CHAs are occluded as protonated form, their structural information, such as atomic coordinates and interactions with the framework remain unknown. Hence, we further investigate the locations of CHAs and host-guest interactions in the as-made SAPO-17 via Rietveld refinement against PXRD data.

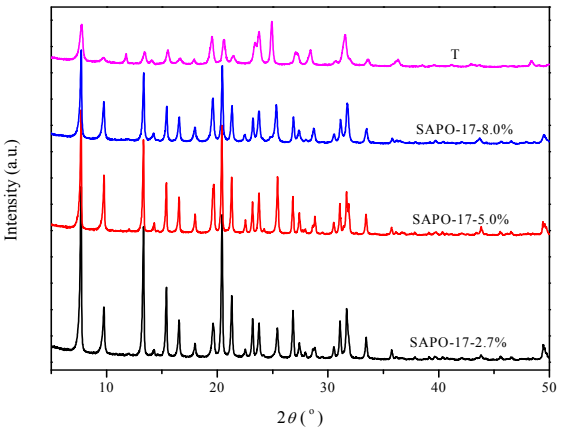

Fig. 2. PXRD patterns of zeolite T and SAPO-17 samples.

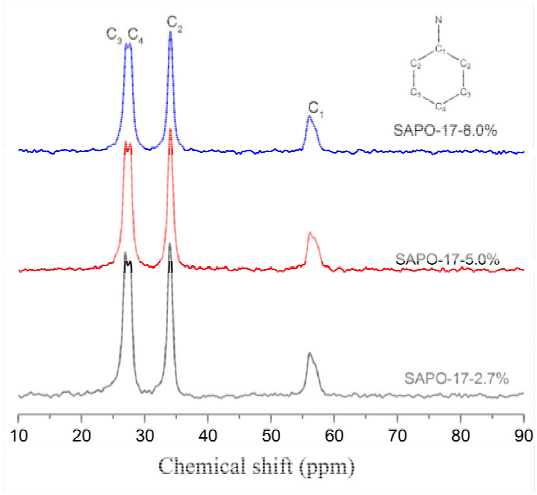

Fig. 3. ^{1}H-^{13}C CP MAS NMR spectra of SAPO-17 samples.

3.2. Rietveld Refinement results of SAPO-17-8.0%

Among the samples synthesized, we choose SAPO-17-8.0% as an example for further structural elucidation. The initial structure model of SAPO-17 was adopted from the International Zeolite Association (IZA). Si was treated and distributed evenly at four T sites. The adopted atomic coordinates of P, Al, and O are further optimized based on the chemical composition, and the experimental unit cell parameters are deduced from LeBail fitting. As the high angle data is not affected significantly by the guest species in the cages, we can search an appropriate scale factor between experimental and simulated data based on the data from 60° to 120° in 2θ. Applying this scale factor to the whole pattern, a difference Fourier map was obtained (Fig. S6). It is clear that each *eri* cage has two clouds of electron densities. Due to the characteristic features of CHA, a six membered ring and an NH_2 group, we can identify the initial positions of CHAs easily based on the difference Fourier map. The simulated annealing algorithm was then employed to determine the initial locations and orientations of CHAs (CHA is considered as a rigid body in this procedure). Finally, the atomic coordinates of P, Al, and O atoms, the zero shift, and the unit cell parameters, etc. are refined. The final Rietveld refinement was converged to R_p = 1.965%, R_{wp} = 2.707%, R_{Bragg} =

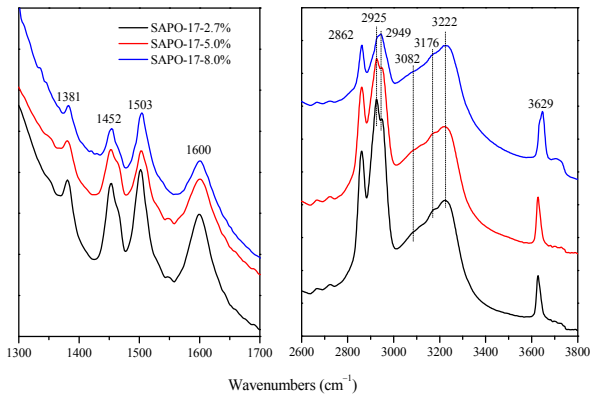

Fig. 4. DRIFT spectra of as-made SAPO-17 samples.

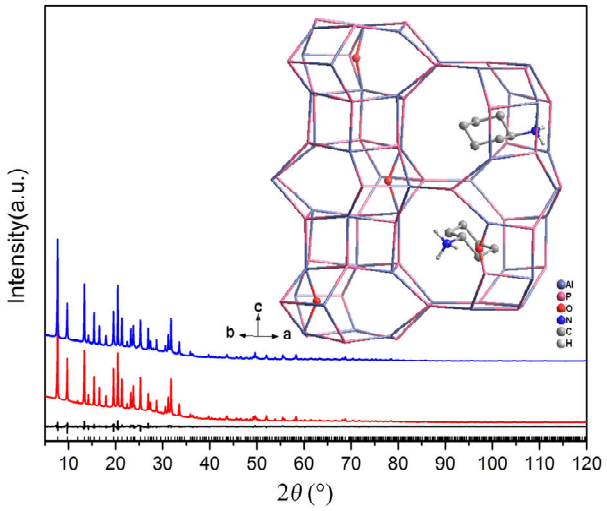

Fig. 5. Final Rietveld refinement plots of SAPO-17-8.0%. The observed, calculated, and difference curves are in blue, red, and black, respectively. The vertical bars indicate the positions of Bragg peaks (Cu $K\alpha1$, λ = 1.5406 Å). The inset is the locations of CHAs and hydroxide groups in *eri* and *can* cages, respectively. For clarity, O and H atoms are omitted, except the special positions including O atoms of OH^- groups in can cages, O atoms forming hydrogen bonds with N atoms, and H atoms coordinating with N atoms.

0.870%, and GOF = 1.699 (as shown in Table S3 and Fig. 5). Additionally, atomic coordinates, inter-atomic distances, and bond angles for the final refinement are provided in Table S4 and S5, respectively. The final refinement reveals that each *eri* cage accommodates two CHAs as deduced from TG (Fig. S2). The NH_3^+ groups of the protonated CHAs point to the 8-ring pore openings and the classical hydrogen-bond N-H…O4 is identified, which indicates that, after the calcination, the proton bonded with O4 will be the Brönsted acid site. SAPO-17-8.0% has OH^- groups located in *can* cages and coordinated to Al1 atoms, as indicated by DRIFT and ^{27}Al NMR.

3.3. Catalytic performance in NH_3-SCR reaction

Inspired by past experiments regarding the Cu loading small-pore SAPO MSs for the NH_3-SCR reaction, we tentatively prepared Cu-SAPO-17 for this reaction. Fig. 6a shows the NO conversion of the fresh Cu-SAPO-17-2.7%-0.42, Cu-SAPO-17-5.0%-0.47, and Cu-SAPO-17-8.0%-0.43. The activities of these three catalysts increase as follows: Cu-SAPO-17-2.7%-0.42 < Cu-SAPO-17-5.0%-0.47 < Cu-SAPO-17-8.0%-0.43. As shown in Fig. 7, the bands at 1440 and 1615 cm^{-1} are assigned to the N-H bending vibration of NH_3 adsorbed on Brönsted acid sites and Lewis acid sites, respectively. The bands at 3189, 3220, 3284, and 3357 cm^{-1} belong to NH_3 adsorbed on the Cu^{2+} ions, the asymmetrical and symmetrical vibration of NH_4^+, and physically adsorbed NH_3, respectively [37]. The Brönsted acid sites of these three catalysts also increase as Cu-SAPO-17-2.7%-0.42 < Cu-SAPO-17-5.0%-0.47 < Cu-SAPO-17-8.0%-0.43. This is further confirmed by NH_3-TPD results (Figs. S7 and S8). In addition, the contents of Cu^{2+} also increase as Cu-SAPO-17-2.7%-0.42 < Cu-SAPO-17-5.0%-0.47 < Cu-SAPO-17-8.0%-0.43 (Table 1). More Brönsted acid sites and Cu^{2+} were beneficial to NH_3-SCR activity [38,39]. Thus, compared with the other two catalysts, Cu-SAPO-17-8.0%-0.43 shows the best NH_3-SCR activity.

Cu-SAPO-17-8.0%-0.43 displays the best activity among these three catalysts. Hence, we exchanged different amounts of Cu^{2+} to SAPO-17-8.0% and tested the influence of Cu contents over the NH_3-SCR. As illustrated in Fig. 6b, Cu-SAPO-17-8.0%-0.22 shows the best NO conversion among these three samples. The decrease of Cu^{2+} contents in Cu-SAPO-17-8.0%-0.11 (Table 1) results in its lower activity in the low-temperature region. Compared with Cu-SAPO-17-8.0%-0.22, the activity of Cu-SAPO-17-8.0%-0.43 decreases in the high-temperature region, which might be attributed to the decrease of its crystallinity framework (Table S6) and a higher Cu content [40]. As mentioned earlier, the HT and LT hydrothermal stabilities of NH_3-SCR catalysts are important to practical applications. Moreover, we also investigated the activities of catalysts aged at 353 K under 10% H_2O/N_2 for 24 h and 973 K under 10% H_2O/air for 16 h to test their LT and HT hydrothermal stabilities, respectively. After HT hydrothermal aging, Cu-SAPO-17-8.0%-0.43 lost most of its activity (Fig. 6c). This is due to the collapse of its crystallinity framework as shown in Fig. S9 and Table S6. After HT hydrothermal aging, Cu-SAPO-17-8.0%-0.22 and Cu-SAPO-17-8.0%-0.11 showed comparable activities and they maintained most of the crystallinity framework (Figs. S10, S11, and Table S6). Considering the fresh and HT hydrothermal aging activity results, Cu-SAPO-17-8.0%-0.22 exhibits the best activity. Thus, when we tested its LT hydrothermal stability as shown in Fig. 6d, it maintains over 90% fresh activity in the low-temperature range (< 523 K) and nearly 100% fresh activity in the high-temperature range (> 523 K).

In order to further understand the properties of Cu-SAPO-17, UV-vis, and EPR were carried out. As shown in Fig.

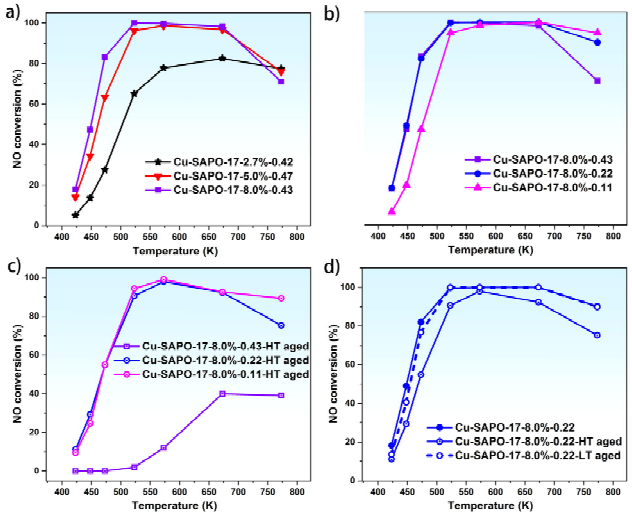

Fig. 6. NH_3-SCR performance of Cu-SAPO-17 a) Fresh activities of Cu-SAPO-17 which have different Si contents but similar Cu/Si Fresh b) and 973 K aged c) activities of Cu-SAPO-17-8.0% with different Cu loading d) Fresh, 973 K aged and 353 K aged activities of Cu-SAPO-17-8.0%-0.22.

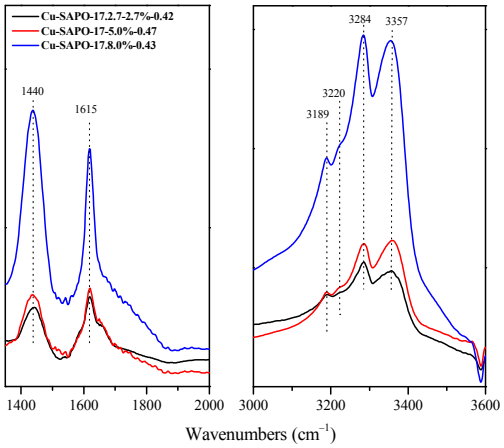

Fig. 7. NH_3-IR spectra of fresh Cu-SAPO-17 samples.

S12, fresh Cu-SAPO-17 catalysts display similar UV-vis spectrum, and they contain not only isolated Cu^{2+} but also Cu cluster and CuO_x. Therefore, we quantified isolated Cu^{2+} by EPR results (Table 1). Cu-SAPO-17 shows one signal of $g_{//}$ = 2.355, $A_{//}$ = 144 G (Fig. S13). Unfortunately, we cannot identify the locations of Cu^{2+} through EPR, only four suitable sites were speculated in the previous literature [17]. We failed to locate the Cu^{2+} through refining the PXRD data of Cu-SAPO-17 sample, due to the low Cu^{2+} contents. Fortunately, we have identified the Brönsted acid sites (bonded with O4) through refining the PXRD data of the as-made SAPO-17. Al and P atoms distribute alternately in AlPO molecular sieves, thus, ignoring the influence of Si island; Si atoms mainly substitute P1 in SAPO-17-8.0%. Considering orientations of O atoms and the charge balance in Cu-SAPO-17, we can deduce the possible locations of Cu^{2+}: site I, adjacent to the 6-ring window joining the *can* cage and *d6r* but displaced into *can* cages; site II, adjacent to the *s6r* joining the *can* and *eri* cage but displaced into *eri* cage (Fig. 8). The accurate locations of Cu^{2+} in Cu-SAPO-17 are still under investigation.

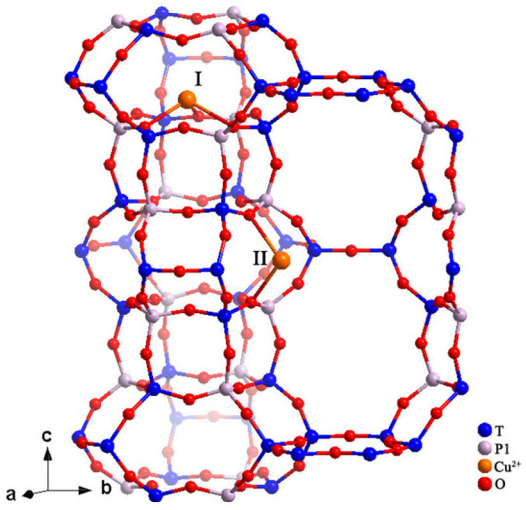

Fig. 8. The possible locations of Cu^{2+} deduced from the distributions of the Brönsted acid.

4. Conclusion

In conclusion, SAPO-17 was hydrothermally synthesized by commercialized cyclohexylamine and their Si contents can be tunable. Rietveld refinement results reveal that CHAs are located in the ellipsoidal *eri* cages and H atoms of NH_3^+ groups formed the hydrogen bond with O4. Finally, SAPO-17 samples were exchanged with Cu in the aqueous solution and tested their NH_3-SCR activities. Cu-SAPO-17-8.0%-0.22 exhibits promising activities even after being aged at 353 K for 24 h or 973 K for 16 h. The methodology regarding the structural elucidation by Rietveld refinement can be utilized in other crystalline porous materials in the near future.

References

[1] L. Zhang, Q. Wu, X. Meng, U. Müller, M. Feyen, D. Dai, S. Maurer, R. McGuire, A. Moini, A.-N. Parvulescu, W Zhang, C. Shi, T. Yokoi, X. Pan, X. H. Bao, H. Gies, B. Marler, D. de Vos, U. Kolb, F. Xiao, *React. Chem. Eng.*, **2019**, 4, 975–985.
[2] A. M. Beale, F. Gao, I. Lezcano-Gonzalez, C. H. F. Peden, J. Szanyi, *Chem. Soc. Rev.*, **2015**, 44, 7371–7405.
[3] Y. Cao, D. Fan, P. Tian, L. Cao, T. Sun, S. Xu, M. Yang, Z. Liu, *Chem. Eng. J.*, **2018**, 354, 85–92.
[4] N. Wilken, K. Wijayanti, K. Kamasamudram, N. W. Currier, R. Vedaiyan, A. Yezerets, L. Olsson, *Appl. Catal. B*, **2012**, 111–112, 58–66.
[5] J. A. Sullivan, J. Cunningham, M. A. Morris, K. Keneavey, *Appl. Catal. B*, **1995**, 7, 137–151.
[6] J. H. Kwak, R. G. Tonkyn, D. H. Kim, J. Szanyi, C. H. F. Peden, *J. Catal.*, **2010**, 275, 187–190.
[7] M. Moliner, C. Franch, E. Palomares, M. Grill, A. Corma, *Chem. Commun.*, **2012**, 48, 8264–8266.
[8] N. H. Ahn, T. Ryu, Y. Kang, H. Kim, J. Shin, I.-S. Nam, S. B. Hong, *ACS Catal.*, **2017**, 7, 6781–6785.
[9] N. Martín, C. Paris, P. N. R. Vennestrøm, J. R. Thøgersen, M. Moliner, A. Corma, *Appl. Catal. B*, **2017**, 217, 125–136.
[10] X. Liu, N. Yan, L. Wang, C. Ma, P. Guo, P. Tian, G. Cao, Z. Liu, *Microporous Mesoporous Mater.*, **2019**, 280, 105–115.
[11] Z. Chen, C. Fan, L. Pang, S. Ming, W. Guo, P. Liu, H. Chen, T. Li, *Chem. Eng. J.*, **2018**, 348, 608–617.
[12] N. Liu, J. Wang, B. Chen, Y. Li, R. Zhang, *Chem. J. Chin. Univ.*, **2016**, 37, 1817–1825.
[13] X.-Q. Liu, S.-h. Li, M.-t. Sun, C.-l. Yu, B.-C. Huang, *Acta Phys. Chim. Sin.*, **2016**, 32, 1236–1246.
[14] A. Lorena Picone, S. J. Warrender, A. M. Z. Slawin, D. M. Dawson, S. E. Ashbrook, P. A. Wright, S. P. Thompson, L. Gaberova, P. L. Llewellyn, B. Moulin, A. Vimont, M. Daturi, M. B. Park, S. K. Sung, I. Nam, S. B. Hong, *Microporous Mesoporous Mater.*, **2011**, 146, 36–47.
[15] J. J. Pluth, J. V. Smith, J. M. Bennett, *Acta Cryst. Sec. C*, **1986**, C42, 283–286.
[16] B. M. Lok, C. A. Messina, R. L. Patton, R. T. Gajek, T. R. Cannan, E. M. Flanigen, US Patent 4440871, **1984**.
[17] A. M. Prakash, L. Kevan, *Langmuir*, **1997**, 13, 5341–5348.
[18] B. Zibrowius, U. Lohse, *Solid State Nucl. Magn. Reson.*, **1992**, 1, 137–148.
[19] I. Girnus, E. Löffler, U. Lohse, F. Neissendorfer, *Collect. Czech. Chem. Commun.*, **1992**, 57, 946–958.

Graphical Abstract

Chin. J. Catal., 2020, 41: 1715–1722 doi: 10.1016/S1872-2067(20)63609-9

Cu-SAPO-17: A novel catalyst for selective catalytic reduction of NO_x

Xiaona Liu, Yi Cao, Nana Yan, Chao Ma, Lei Cao, Peng Guo *, Peng Tian *, Zhongmin Liu *
Dalian Institute of Chemical Physics, Chinese Academy of Sciences; University of Chinese Academy of Sciences; Ningbo University; Dalian University of Technology

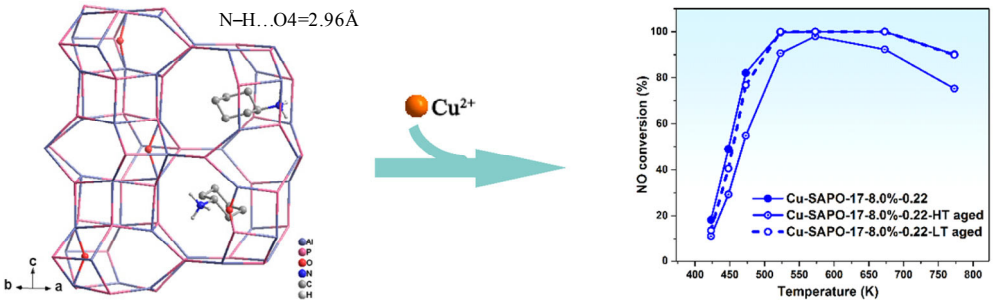

Cu-SAPO-17 was utilized as a novel NH_3-SCR catalyst for the first time, which shows promising low- and high- temperature hydrothermal stabilities. The possible Cu^{2+} sites were further deduced from Rietveld refinement results.

[20] Q. Liu, N. C. O. Cheung, A. E. Garcia-Bennett, N. Hedin, *ChemSusChem*, **2011**, 4, 91–97.
[21] Q. Gao, S. Li, R. Xu, *J. Chem. Soc., Chem. Commun.*, **1994**, 1465–1466.
[22] A. Tuel, C. Lorentz, V. Gramlich, C. Baerlocher, *C. R. Chimie*, **2005**, 8, 531–540.
[23] E. W. Valyocsik, R. Von Ballmoos, *US Patent 4778780*, **1988**.
[24] M. J. Maple, C. D. Williams, *Dalton Trans.*, **2007**, 4175–4181.
[25] A. B. Pinar, L. Gómez-Hortigüela, L. B. McCusker, J. Pérez-Pariente, *Chem. Mater.*, **2013**, 25, 3654–3661.
[26] L. Gómez-Hortigüela, F. Corà, C. R. A. Catlow, J. Pérez-Pariente, *J. Am. Chem. Soc.*, **2004**, 126, 12097–12102.
[27] L. Marchese, A. Frache, E. Gianotti, G. Martra, M. Causà, S. Coluccia, *Microporous Mesoporous Mater.*, **1999**, 30, 145–153.
[28] F. Fan, Z. Feng, K. Sun, M. Guo, Q. Guo, Y. Song, W. Li, C. Li, *Angew. Chem. Int. Ed.*, **2009**, 48, 8743–8747.
[29] M. B. Park, Y. Lee, A. Zheng, F.-S. Xiao, C. P. Nicholas, G. J. Lewis, S. B. Hong, *J. Am. Chem. Soc.*, **2013**, 135, 2248–2255.
[30] B. Han, C.-H. Shin, S. J. Warrender, P. Lightfoot, P. A. Wright, M. A. Camblor, S. B. Hong, *Chem. Mater.*, **2006**, 18, 3023–3033.
[31] S. Smeets, S. I. Zones, D. Xie, L. Palatinus, J. Pascual, S.-J. Hwang, J. E. Schmidt, L. B. McCusker, *Angew. Chem. Int. Ed.*, **2019**, 58, 13080–13086.
[32] N. Yan, L. Wang, X. Liu, P. Wu, T. Sun, S. Xu, J. Han, P. Guo, P. Tian, Z. Liu, *J. Mater. Chem. A*, **2018**, 6, 24186–24193.
[33] S. B. Hong, E. G. Lear, P. A. Wright, W. Zhou, P. A. Cox, C.-H. Shin, J.-H. Park, I.-S. Nam, *J. Am. Chem. Soc.*, **2004**, 126, 5817–5826.
[34] S. Zhong, S. Song, B. Wang, N. Bu, X. Ding, R. Zhou, W. Jin, *Microporous Mesoporous Mater.*, **2018**, 263, 11–20.
[35] U. Lohse, Loffler, E, Kosche, K, Janchen, J, Parlitz, B, *Zeolites*, **1993**, 13, 549–556.
[36] X. Xiang, M. Yang, B. Gao, Y. Qiao, P. Tian, S. Xu, Z. Liu, *RSC Adv.*, **2016**, 6, 12544–12552.
[37] Y. Cao, D. Fan, L. Sun, M. Yang, L. Cao, T. Sun, S. Xu, P. Tian, Z. Liu, *Chem. Eng. J.*, **2019**, 374, 832–839.
[38] T. Yu, J. Wang, M. Shen, W. Li, *Catal. Sci. Technol.*, **2013**, 3, 3234–3241.
[39] S. A. Bates, A. A. Verma, C. Paolucci, A. A. Parekh, T. Anggara, A. Yezerets, W. F. Schneider, J. T. Miller, W. N. Delgass, F. H. Ribeiro, *J. Catal.*, **2014**, 312, 87–97.
[40] J. Tang, M. Xu, T. Yu, H. Ma, M. Shen, J. Wang, *Chem. Eng. Sci.*, **2017**, 168, 414–422.

Cu-SAPO-17：一种新颖的NO_x选择性催化还原催化剂

刘晓娜[a,b], 曹 毅[a,c], 闫娜娜[a,b], 马 超[a,b,d], 曹 磊[a], 郭 鹏[a,*], 田 鹏[a,#], 刘中民[a,$]
[a]中国科学院大连化学物理研究所, 甲醇制烯烃国家工程实验室, 国家能源低碳催化与工程研发中心, 洁净能源国家实验室(筹), 辽宁大连116023
[b]中国科学院大学, 北京100049
[c]宁波大学材料科学与化学工程学院, 浙江宁波315211
[d]大连理工大学张大煜学院, 辽宁大连116024

摘要: 在柴油机排放后处理系统中, 颗粒捕捉器经常放在氨气选择性催化还原(NH_3-SCR)催化剂附近. 在颗粒捕捉器的再生环节中, 其需要加热到873 K以上. 同时, 在柴油机存储和冷启动阶段, NH_3-SCR催化剂需要暴露在低温(373 K以下)条件

下. 因此, NH_3-SCR催化剂需要同时具备优异的高温水热稳定性和低温水热稳定性. 在现有NH_3-SCR催化剂中, 铜交换的磷酸硅铝(SAPO)分子筛由于具有优异的高温水热稳定性而受到广泛关注. 到目前为止, 在现有41种SAPO分子筛中, 仅有Cu-SAPO-34, Cu-SAPO-18, Cu-SAPO-35, MnO_x-SAPO-11和Cu-SAPO STA-7被应用到NH_3-SCR反应中. 在这些SAPO分子筛中, 除SAPO-11外, 其他分子筛都具有小孔大笼的特征. 然而, SAPO分子筛在NH_3-SCR反应中的广泛应用一直受到其低温水热稳定性的限制. 因此, 研究者们一直致力于研发其他具有小孔大笼特征的SAPO分子筛, 以实现低温水热稳定性和高温水热稳定性兼备.

本文报道了一个新颖的Cu-SAPO-17催化剂的合成, 并首次将其应用于NH_3-SCR反应中. SAPO-17具有三维8 × 8 × 8孔道结构, 由沿着*c*轴的*eri*笼和*can-d6r*构成. 首先采用廉价的环己胺(CHA)作为模板剂制备SAPO-17原粉, 随后对SAPO-17原粉进行铜离子交换和焙烧, 得到Cu-SAPO-17催化剂. 通过优化催化剂的硅含量和铜含量, 我们发现Cu-SAPO-17-8.0%-0.22催化剂表现出优异的低温水热稳定性和高温水热稳定性. 该催化剂在353 K和10% H_2O的氮气气氛下老化24 h后(低温水热老化), 可以保持90%以上的新鲜活性; 在973 K和10% H_2O的空气气氛下老化16 h后(高温水热老化), 在473 K下仍然可以达到50%以上的NO转化率. 通过X射线粉末精修(Rietveld精修)SAPO-17-8.0% (未焙烧)确定了模板剂环己胺的落位、分子筛中的主客体相互作用以及Brönsted酸位点分布. 精修结果显示: 1)一个*eri*笼子中包含两个质子化的环己胺; 2)环己胺上的N原子与骨架上的O4形成了经典的氢键(N–H...O4 = 2.96 Å). 这意味着催化剂焙烧之后, 与氢键相连的O4即是Brönsted酸位点. 因为O4与P1相连, 所以在忽略硅岛的影响时, 可以认为Si在SAPO-17-8.0%中主要取代P1位点. 结合EPR结果, 我们推测出两种Cu^{2+}的可能落位.

关键词: SAPO-17分子筛; Rietveld精修; 主客体相互作用; 氨气选择性催化还原(NH_3-SCR); 水热稳定性; Cu^{2+}落位

收稿日期: 2020-02-21. 接受日期: 2020-03-29. 出版日期: 2020-11-05.

*通讯联系人. 电话: (0411)84379149; 传真: (0411)84379289; 电子信箱: pguo@dicp.ac.cn

#通讯联系人. 电话: (0411)84379218; 传真: (0411)84379289; 电子信箱: tianpeng@dicp.ac.cn

$通讯联系人. 电话: (0411)84379998; 传真: (0411)84379289; 电子信箱: liuzm@dicp.ac.cn

基金来源: 国家自然科学基金(21972136, 21676262, 21606221, 21991091); 中国科学院前沿科学重点研究计划(QYZDB-SSW-JSC040).

本文的电子版全文由Elsevier出版社在ScienceDirect上出版(http://www.sciencedirect.com/science/journal/18722067).